Evolution of the transport properties of soil aggregates and their relationship with soil organic carbon following land use changes

Feng Wang[1], Xiaoxian Zhang[2], Andrew L Neal[3], John W Crawford[4], Sacha J. Mooney[5], Aurélie Bacq-Labreuil[5]

[1]Farmland Irrigation Research Institute, Chinese Academy of Agricultural Sciences, Xinxiang 453003, Henan Province, China.

[2] Department of Sustainable Agricultural Sciences, Rothamsted Research, Harpenden, AL5 2JQ, UK.

[3] Department of Sustainable Agriculture Sciences, Rothamsted Research, North Wyke, EX20 2SB, UK

[4] Adam Smith Business School, University of Glasgow, West Quadrangle, Glasgow G12 8QQ. UK

[5] Division of Agriculture & Environmental Sciences, School of Biosciences, University of Nottingham, Sutton Bonington Campus, Leicestershire LE12 5RD, UK.

Abstract

Aggregates are functional units to describe the impact of soil structural changes on physical and biogeochemical processes in soil. Both incubation and field experiments have shown that changing agricultural practices could reshape the intra-aggregate structure in a matter of days, but most such data were obtained from a single time-point and it is hence impossible to interpret that such a change was just a temporal transition or the new equilibria towards which the aggregates had evolved following the management changes. Understanding this is indispensable as intra-aggregate structure and its ability to transport substrates modulate all biogeochemical processes involved in soil carbon and nutrient cycle. This paper investigates this using soil samples archived from a reversion experiment initiated in 2008 at Rothamsted Research (UK), where parts of a plot that had been fallow since the 1950s were converted to wheat or grass in 2008. We used X-ray Computed Tomography images, acquired at voxel size 1.5µm, of aggregates in the archived soils to investigate the evolution of transport property of the aggregates over time, as well as its relationship with soil organic carbon (SOC). We also evaluated the development of pore connectedness following the conversion. The results show that the transport ability of the aggregates and SOC are positively correlated at significant level, and noticeable changes in porosity of the connected pores and their ability to transport substrates did not emerge until sixth year after the conversion. Ten years after the conversion, there was still no sign of the porosity of the connected pores and the bulk diffusion coefficient to plateau. In addition, we found the conversion to grass changed the intra-aggregate pore geometry significantly in that the bulk diffusion coefficients of their aggregates trends with their porosities in a way differing significantly from those for the bare fallow and arable treatments. All these suggest that the intra-aggregate reconfiguration following the conversion is a slow process, and that the ability of pore space to transport substrates is more important than the habitat they provide in SOC stabilisation.

Keywords: Long-term experiment; land use change; intra-aggregate structure; bulk diffusion coefficient; soil organic carbon.

1. Introduction

Soil aggregates are the functional units of soil structure which impact on physical and biogeochemical processes in soil despite the ongoing debate over the applicability of this approach (Kravchenko et al., 2019a; Wang et al., 2019). They play a critical role in stabilizing organic carbon and retaining water and nutrients for plants and microbes to take up (Ananyeva et al., 2013; Angst et al., 2017; Jastrow et al., 1996). Although the abiotic and biotic factors responsible for formation and disintegration of the aggregates have been well documented (Totsche et al., 2018), the length of time required for newly formed aggregates to reach new equilibrium state following land management change is unclear due to the limited field experiments which should run long enough to assess temporal transitions. Incubation experiments have consistently shown that adding exogenous carbon resulted in soil re-aggregating in a matter of days (Crawford et al., 2012; Rabbi et al., 2018), but it is unclear that such rapid changes represent a transition or a new equilibrium state to which the aggregates had evolved as a response to the environmental changes.

Soil aggregation is a multifaceted process mediated by a myriad of abiotic and biotic processes operating over a hierarchical scale. It is initiated by organo-mineral complexes and extracellular polymeric substances binding minerals into micro-aggregates (Christensen, 2001), followed by a further agglomeration by fungi hyphae, roots and other decomposed organic matter to form macroaggregates (Totsche et al., 2018). As these processes are modulated by soil organic matter (Six et al., 2000), it is rational to assume that soil aggregation may not reach a new equilibrium state before soil organic matter (SOM) stabilizes following a land management change (Young and Crawford, 2004). This is manifested by recent findings that soil organic carbon (SOC) stabilization is strongly associated with aggregation and that disintegration of aggregates leads to a soil carbon loss (Dungait et al., 2012; Schmidt et al., 2011).

Soil is a dynamic system and there is currently no consensus regarding the turnover time of soil aggregates. A paucity of available studies suggested that the turnover time can

vary from 8 to 88 days, depending on aggregate size (Totsche et al., 2018). This is, however, inconsistent with the turnover time of soil carbon which could be >100 years (Hemingway et al., 2019; John et al., 2005). A change in cultivation has been found to slowly shift aggregate fractions (Lobe et al., 2011), but it is unknown if the associated intra-aggregate structure also evolves at the same rate. This is a critical knowledge gap and understanding it is important, because soil microbial communities live within those pores, and a rearrangement of intra-aggregate pores would alter the accessibility of water and substrates to microbes (Ananyeva et al., 2013; Juarez et al., 2013), thereby changing the response of SOC to global warming.

The aim of this paper is to address this lack of understanding using a reversion experiment at Rothamsted Research (UK), where parts of experimental plots fallowed in the 1950s were replanted with wheat or grass in the late 1990s. X-ray images of intact aggregates in the soil samples archived since 2008 were used to calculate the change in porosity of connected pores, as well as the ability of the aggregates to diffuse substrates. Considering that the organo-mineral complexes account for a significant portion of SOC in dry soils and that SOC persistence depends on the ability of aggregates to transport substrates and enzymes, we also analysed the variation in SOC with porosity and bulk diffusion coefficient of the aggregates to elucidate that it is the habitat provided by the pores or their ability to move substrates that affects SOC more.

2. Materials and methods

2.1. Experiment and soil images

Details of the reversion experiment are available in the e-RA database managed by Rothamsted Research (Perryman et al., 2018), and in the literature (Bacq-Labreuil et al., 2020; Hirsch et al., 2017). The experimental site had been permanent grass since at least 1883 and in 1949 some plots on the site were converted into continuous arable and arable-grass alternation respectively. In 1959, a long-term bare fallow was established (Gregory et al., 2016). In 2008, plots of soil managed as bare fallow were converted to arable and grass management (Hirsch et al., 2017). Since then, soils have been sampled annually from each

96 treatment and then archived. In this paper, we investigated the archived soils sampled from
97 the plots that were converted to winter wheat (*Triticum aestivum* L.), and a mixture of fescue
98 (*Festuca pratensis* L.), Timothy grass (*Phleum pratense* L.) and white clover (*Trifolium*
99 *repens* L.), respectively, in 2008, with the continuing bare fallow taken as the control; both
100 bare fallow and arable plots were annually ploughed. The archived soils sampled in 2008-
101 2018 were sieved (2mm mesh size) first, and intact aggregates retained in the sieve were
102 scanned using a Phoenix Nanotom X-ray Computed Tomography system at a voxel size of
103 1.5 μm. All image stacks were cropped to cuboids comprising 650x480x400 voxels, with
104 nine replicates in each treatment. Detailed procedures for acquiring and processing the
105 images, as well as their geometrical parameters were presented previously (Bacq-Labreuil et
106 al., 2021). In this paper, we focused on evolution of the connected pores and the transport
107 properties, as well as their relationship with SOC following the conversions. Since
108 biogeochemical reactions continue after the soils were sampled and archived, we used data
109 on SOC from the e-RA rather than re-measure it from each aggregate.

110 **2.2. Connected pores**

111 Previous analysis of the images of soil samples taken in 2015 from the fallow plot
112 revealed that following the fallow in1959, the porosity of connected pores has been reduced
113 substantially and the reduction increased with sample size (Bacq-Labreuil et al., 2018). As
114 the conversions in 2008 has gradually increased the intra-aggregate porosity (Bacq-Labreuil
115 et al., 2021), we anticipated that the conversions would have an inverse effect: enhancing
116 the possibility of a pore to joint with its adjacent pores to form clusters, and the length of the
117 clusters grew with time. However, the archived samples were very fragile and there are no
118 aggregates which are larger than what we managed to scan. Therefore, instead of studying
119 the variation in cluster lengths, we took the advantage of the cuboid soil images, calculating
120 the change in pores in clusters with fixed lengths that stretched to 0.60 mm and 0.975 mm
121 respectively; the calculation was based on the method we used previously (Zhang et al.,
122 2016b). In what follows, the volumetric fraction of pores in each type of the clusters will be
123 called porosity unless stated otherwise.

2.3. Diffusion coefficient

The effective diffusion coefficient of each aggregate was calculated from the lattice Boltzmann simulation by mimicking substrate diffusion through its pore space. Details of the method are given in the Appendix. Solute diffusion through the pore space was driven by a concentration gradient generated by imposing a high concentration on one side and a low concentration on its opposite side of the aggregate; the other four sides were treated as periodic boundaries. The diffusion was simulated to steady state – deemed to have reached once the absolute relative difference between concentrations at two time points separated by 300 time steps was less than 10^{-6} for all voxels. After the diffusion was at steady state, we sampled both solute concentration and diffusive flux in all voxels and then spatially averaged them across each section perpendicular to the imposed concentration gradient direction to generate an average concentration profile and an average diffusive flux profile; they were assumed to follow Fick's law and used to calculate the effective diffusion coefficient. Considering that the diffusion coefficient is direction-dependent, for each aggregate we calculated its diffusion coefficient in all three directions. When the concentration gradient was generated in the x direction, for example, the average diffusive flux and concentration are linked by

$$Q_x = -D_e \frac{\partial C}{\partial x}, \tag{1}$$

where C and Q_x are the average concentration and diffusive flux across each section perpendicular to the x direction, respectively, D_e is the effective diffusion coefficient describing the ability of the pores to diffuse solute. Due to mass-conservation constraint, the average diffusive flux Q_x is constant when diffusion is in steady state. From Eq. (1), we can calculate the effective diffusion coefficient D_e as follows:

$$D_e = \frac{L_x}{N} \frac{\sum_{i=1}^{N} j_x\left(x_i, y_i, z_i\right)}{C_0 - C_1}, \tag{2}$$

where L_x is the length of the sample in the x direction, N is the number of all pore voxels, $j_x(x_i, y_i, z_i)$ is the diffusive flux component in the x direction at voxel coordinated at (x_i, y_i, z_i),

C_1 and C_0 are the high and low concentrations used to generate the concentration gradient in the x direction respectively. We also calculated the tortuosity based on the simulated diffusive flux in all voxels using the method we developed (Zhang et al., 2021b):

$$\tau = \frac{\sum_{i=1}^{N} \left\| \boldsymbol{J}(\boldsymbol{x}_i) \right\|}{\sum_{i=1}^{N} J_x\left(\boldsymbol{x}_i\right)}, \quad (3)$$

where $\boldsymbol{J}(x_i, y_i, z_i)$ is the diffusive flux vector at voxel coordinated at (x_i, y_i, z_i), and other variables are the same as those in Eq.(2). Physically, τ is the ratio between the average length of all diffusing lines along which the solute moves from the inlet face to the outlet face and the Eulerian distance between the two faces.

2.4. Statistical analysis

Statistical comparison of the mean between different treatments and time was assessed by the analysis of variance (ANOVA), and post-hoc pairwise comparisons were performed using the Duncan's multiple range test with the difference considered significant at $p < 0.05$. The difference in the variation of diffusion coefficient with porosity between different treatments was calculated using the analysis of covariance (ANOCOVA). All analyses were calculated using Matlab. The difference in regression curves for data between treatments was also calculated using Matlab.

3. Results

As an illustration, Figure 1 compares how the intra-aggregate pore geometry had evolved over the 10-year period after the conversion in 2008. Since molecular diffusion coefficient depends on solute and temperature, in what follows we will normalize the effective diffusion coefficient of each solute by its molecular diffusion coefficient, D, in water at the same temperature, i.e., $D_e' = D_e / D$.

3.1. Evolution of pore connectedness

Figure 2 compares the change in the volumetric fraction of pores (referred to as porosity thereafter) in the two types of clusters stretching to 0.60 and 0.98mm respectively. For the continuous bare fallow, the porosity in the clusters 0.975mm long was consistently lower

than that in the clusters 0.60 mm long (except in 2010), though not at significant level. The porosity of the two types of clusters fluctuated because of soil heterogeneity and neither showed an identifiable trend over the 10-year period. Conversion to grass or wheat did not result in a noticeable change in the porosity of the two types of clusters in the first two years, but there was a sign that the impact, though not at significant level, started to emerge from the fourth year. Significant change appeared 10 years after the conversion.

There are two intriguing differences between the wheat and grass conversions. The first one is that the conversion to grass increased the porosity of the two types of clusters faster than the conversion to wheat. For example, four years after the conversion, the porosity of the two types of clusters in the grass treatment was approximately 6%, while the porosity of the wheat treatment was only 3%; this twofold difference continued into the 10^{th} year. The second one is that as time elapsed, especially from the seventh year, the conversion to grass appeared to have made the aggregates more homogenous as evidenced from the standard deviations of the porosity of both types of clusters, which are lower than that in the wheat treatment (Figures 2B and 2C).

3.2. Change in bulk diffusion coefficient

The bulk diffusion coefficients calculated from the three directions in each sample differed slightly, and the degree of the anisotropy varied between aggregate and the treatment. Because all soil samples were sieved before being archived, different directions in the soil images did not represent their orientations in the field. No significant difference was identified between the treatments over the 10-year period. Therefore, in what follows we will use the average of the three diffusion coefficients of each sample to describe its ability to diffuse substrates.

The diffusion coefficient of soils has been expressed in different ways. One is effective diffusion coefficient to describe the reduced ability of the pore space to transport solute due to the tortuous pathways for the solute to move through as calculated from Eq. (2). The second one is bulk diffusion coefficient, D_b, representing the bulk solute flux diffusing cross a unit cross-section, including both pore and solid phases, under a unit concentration gradient.

Their relationship is $D_b = \varepsilon D_e$ with ε being the porosity. In the following analysis, we will use the bulk diffusion coefficient as it is more appropriate to quantify the ability of soil to move substrates; it was also normalized by molecular diffusion of the solute in water: $D' = \varepsilon D_e'$.

Figure 3 shows the changes in the normalized average bulk diffusion coefficient of the aggregates with treatment and time. The conversion to wheat led to a slight drop in the diffusion coefficient in the first three years, followed by an increase from the sixth year, though not at significant level ($p>0.05$). It is unknown that this initial drop was due to soil heterogeneity or the consequence of the conversion. A similar phenomenon was also observed from the grass conversion, where the average diffusion coefficient did not show a noticeable change in the first three years but started to increase steadily from the fourth year at significant scale ($p<0.05$) compared to that in 2008. Ten 10 years after the conversion to grass, the ability of the aggregates to diffuse substrates differs significantly from the aggregates in the other two treatments ($p<0.05$). One interesting result is that converting the fallow to grass for 10 years increased the intra-aggregate porosity by twofold compared to the conversion to wheat, while its associated diffusion coefficient increased by threefold, because the ability of a soil to diffuse substrates depends on the combination of its porosity and how pores of different sizes are connected spatially. The aggregates in the wheat treatment appeared to have more pore bodies whose contribution to conducting substrates is not proportional to their volume.

The porosity we analysed is image-porosity for pores >1.5μm. As such, the porosity of connected intra-aggregate pores in the fallow and arable treatments is low, varying from 0.015% to 0.06%. This is close to the critical porosity below which soil would become impermeable. It is well established in percolation theory that when the porosity of a porous material is close to the critical porosity, its ability to transport substrates increases with the porosity in a power-law function (Pabst and Gregorova, 2006). This is why the bulk diffusion coefficient of the grass aggregates is higher than that of the arable and fallow aggregates.

3.3. Relationship with soil organic carbon

The aggregates were taken from archived samples without SOC measurement. Given that biogeochemical reactions continue and SOC in the archived samples was no longer the same as the SOC in the field when the soils were sampled, we used the total SOC routinely measured for each treatment as a proxy in the following analysis (Hirsch et al., 2017). This is an approximation but rational, as approximately 90% of SOC was reported to be inside aggregates (Totsche et al., 2018), and SOC is significantly correlated to aggregate-associated SOC (Guo et al., 2020). The initial aim of imaging these achieved samples was to investigate their intra-aggregate structural evolution. Considering that soil structural change is a slow process, the time interval between the samples we imaged was 2-3 years. The total SOC in the routine measurement was analysed using the LECO method, and the results were given in average which are available up to 2012. The change of total SOC in different treatments and the methods to measure it are available in the literature (Hirsch et al., 2017). As we aim to evaluate the relationship between SOC and soil physical properties, we pooled all results in the analysis. Figure 4 shows the impact of SOC on porosity and the average bulk diffusion coefficient of the aggregates taken from all treatments over the 10-year period.

4. Discussion

4.1. Pore connection and diffusion coefficient

The ability of aggregates to transport substrates is modulated by their intra-aggregate pore structure. For aggregates with similar pore geometry, the relationship between their effective diffusion coefficient and porosity follows the same scaling-law (Neuman, 1990). While the aggregates taken from the same treatment are heterogeneous, the relationship between their diffusion coefficient and intra-aggregate porosity can still be used to interpret to what extent the intra-aggregate pore structures under different treatments are geometrically similar. For each treatment, we pooled the results of all aggregates in different years and fitted the change in their bulk diffusion coefficient with porosity to a power-law function as shown in Figure 5. The data in each graph are scattered, yet there is a significant

correlation between porosity and bulk diffusion with $R^2>0.87$ and $p<10^{-7}$ for all three treatments.

The exponent in the power-law function for the aggregates in the wheat treatment was 1.53, more similar to the exponent associated with the bare fallow aggregates (1.48) than to 1.72 - the exponent for the grass aggregates. Analysis of the covariance found that the variation in diffusion coefficient with porosity for the grass treatment differs significantly from that for the fallow and arable treatments ($p<0.05$), indicating that the intra-aggregate pore spaces in the wheat and fallow treatments are more geometrically similar to each other than to the grass treatment. Continuously growing grass for 10 years increased the transport ability of its aggregates by threefold compared to planting with wheat (Figure 3), much higher than the twofold difference between their porosities (Figure 2), suggesting that the grass not only increased the pore space but also reshaped how the pores were connected spatially. Tortuosity is a parameter to characterize the complexity of pore space for fluid and substrates to move through (Zhang et al., 2021a), and Figure 6 compares the change in tortuosity with time and treatment. The conversions to wheat and grass gradually altered the porosity and bulk diffusion coefficient of the aggregates, and the changes became significant from the sixth year (Figures 2, 3). In contrast, their tortuosity was comparable, indicating that the diffusing lines along which the solute moved in the aggregates did not differ from each other significantly ($p>0.05$). On average, the tortuosity of the grass aggregates is the least. All these are consistent with our recent findings that for self-organised soil, its tortuosity for a specific transport process is only loosely correlated to its porosity (Zhang et al., 2021b).

Both the bare fallow and arable plots are ploughed annually, but the tillage alone was unlikely to have disintegrated the aggregates. We cannot rule out the impact of root penetration in the wheat and grass treatments, but the recent finding is that plant roots prefer to grow in loose soil and large pores (Atkinson et al., 2020; Zhou et al., 2020); SEM analyses of aggregates sampled from cropped soils also failed to identify signs of fresh and decomposed roots (Bhattacharyya et al., 2021). As the voxel size was 1.5μm – a scale relevant to microbial activity, microbial and biogeochemical processes were therefore the

likely mechanisms underlying the observed inter-aggregate structural changes following the conversions (Totsche et al., 2018). An early study on the same experimental site found that four years after the conversion, both microbial biomass and abundance of mesofauna increased considerably, especially mesofauna whose numbers increased by about 50-fold (Hirsch et al., 2017). It was estimated that at Rothamsted, carbon input to the soil from grass and arable was approximately 4.5 T ha^{-1} y^{-1} and 1.4 T ha^{-1} y^{-1}, respectively (Johnston et al., 2009). Microbial decomposition of these organic carbons had reshaped the intra-aggregate structure, and the difference in carbon inputs and microbial diversity, more diverse in the arable treatment than in the grass treatment (Hirsch et al., 2017), resulted in the difference in the intra-aggregate structural changes between the treatments.

4.2. Relationship with soil organic carbon

Aggregation and aggregate stability are modulated by microbial decomposition of SOM (Six et al., 2000; Tisdall and Oades, 1982; Tripathi et al., 2014), and in return, microbial activity also reshapes the intra-aggregate structure (Ananyeva et al., 2013; Rabbi et al., 2016; Rabbi et al., 2020; Zhou et al., 2013). Experimental results have consistently shown that adding carbon can increase soil porosity in a matter of days (Crawford et al., 2012; De Gryze et al., 2006), and that aggregate porosity and SOC are positively correlated (Bhattacharyya et al., 2021; Crawford et al., 2012; De Gryze et al., 2006; Rabbi et al., 2020). However, it remains obscure that it is the habitat provided by the increased pore space or the improved ability of the pore space to move substrates that boosts microbial metabolism and consequently improves SOC stabilization. Both porosity and bulk diffusion coefficient are positively correlated with SOC (Figure 6), yet it is the bulk diffusion coefficient that correlates to SOC at significant level ($p<0.05$). In contrast, the porosity and SOC are indeed correlated, consistent with the literature results (Bhattacharyya et al., 2021), but not at significant level ($p>0.05$). As most SOC stabilized in soil is decomposition intermediates of SOM mediated by extracellular enzymes (Kravchenko et al., 2019b; Sainte-Marie et al., 2021), and most pores in soil are devoid of microbes and substrates (Nunan et al., 2003;

313 Young and Crawford, 2004), Figure 4 suggests that the ability of soil to move substrates is
314 more important than its porosity in stabilizing SOC.
315 The role of aggregates in protecting SOC has been well documented (Lobe et al., 2011;
316 Wang et al., 2020). The converging view is that separating SOC from microbes and
317 extracellular enzymes inside the aggregates is the dominant mechanism preventing SOC
318 from decomposition (Wiesmeier et al., 2019); plant inputs need to be converted into
319 microbial residues before being stabilized through physical/chemical adsorptions or
320 entrapment in small pores inaccessible to microbes and enzymes (Gillabel et al., 2010;
321 Kallenbach et al., 2016). It is hence important for pores (>1μm) accessible to microbes to be
322 aerobic so as to boost microbial metabolism while in the meantime moving the
323 decomposition intermediates into microaggregates to escape further decomposition
324 (Kravchenko et al., 2019b; Yang et al., 2021). Having a hierarchical structure with a wide
325 pore-size distribution is hence critical to enhancing SOC sequestration as seen from the
326 aggregates in the grass treatment (Bacq-Labreuil et al., 2018; Bacq-Labreuil et al., 2021).
327 Most pool-based SOC models assume SOM decomposition is predominantly driven by
328 oxygen and that reducing oxygen supply restricts SOM decomposition (Bauer et al., 2008;
329 Davidson et al., 2000; Hursh et al., 2017). In such models, the roles of oxygen and soil water
330 content are described collectively by a moisture function (Skopp et al., 1990; Yan et al.,
331 2018). Our results do not appear to fully support this. Terrestrial soils in drylands are
332 hierarchically structured, with inter-aggregate pores larger than 40μm remaining dry in most
333 seasons while the intra-aggregate pores retain water and dissolved nutrients (Li et al., 2018).
334 As the ability of soil to dissolve and transport gaseous oxygen from the inter-aggregate
335 pores into the intra-aggregate pores controls aeration in the aggregates, it is reasonable to
336 assume that the greater the diffusion coefficient of the aggregates is, the more aerobic the
337 soil would be. This suggests that more SOM should be decomposed when soil aggregates
338 are more permeable based on the pool-based models. While different mechanisms combine
339 to modulate SOM decomposition, an important process in SOC stabilization is the organo-
340 mineral complexes (Hemingway et al., 2019; Lehmann et al., 2020). Organo-mineral

complexes form under aerobic conditions and could dissolve by microbially-induced reduction of iron and manganese under anaerobic conditions. As anoxic microsites prevail in aggregates even when soil is dry (Keiluweit et al., 2016), our results suggest that it is important to maintain aggregates in soils partly aerobic in order to improve their carbon sequestration.

Incubation and field experiments have both shown that a change in land management alters aggregate fractions and reshapes the intra-aggregate structure, thereby resulting in SOC loss or gain (Cooper et al., 2021; Gregory et al., 2016; Helliwell et al., 2014; Jensen et al., 2020; Lobe et al., 2011; Rabbi et al., 2016). However, most of these were obtained at one time-point and thus cannot inform if and how the intra-aggregate structures and their transport ability evolve. While our reversion experiment spanned only 10 years, it is one of the most sophisticated datasets available with simultaneous measurements of intra-aggregate structure, SOC and other biogeochemical processes (Hirsch et al., 2017; Jensen et al., 2019; Neal et al., 2020; Redmile-Gordon et al., 2020). The results obtained from this work offer new insights into how intra-aggregate structure evolves following land management change, as well as the consequence for SOC dynamics.

4.3. Slow intra-aggregate structural change

Change in agricultural practices leads soils to restructure across various scales (Naveed et al., 2014; Rabbi et al., 2020; Tripathi et al., 2014). Our results corroborate this but further show that such a structural change is a slow process and does not appear to have reached a new equilibrium state even after one decade. Why the structural change is so slow and how the change progresses is poorly understood. If the turnover time of aggregates is less than a few months and the aggregates are constantly disintegrated and formed as some experiments have suggested (Totsche et al., 2018), the interior structure of the aggregates sampled at different years from the same treatment should be comparable. This is not corroborated by our results which reveal that the volume of connected pores in the aggregates and their ability to transport substrates remained almost unchanged in the first four years, and they then increased steadily from the sixth year after the conversion; in the

10-year period, they did not show any signs of levelling off (Figures 2-3). While we cannot rule out that the turnover time of some aggregates is short, this is unlikely to be the dominant process as Figures 2-5 show that, following the conversion, the aggregates became increasingly more porous and conductive. Since all soil samples were sieved and air-dried before being archived, the aggregates that do not collapse 10 years after the desiccation must be very stable and are unlikely to have a turnover time of a few months only. Therefore, the most likely mechanisms are that the aggregates remained largely intact, and their interior pore geometry was slowly reconstructed. One possible driving force for such a slow reconstruction is the alternate formation and dissolution of organo-mineral complexes induced by the redox inside the aggregates which constantly changes with soil water (Keiluweit et al., 2016). This is also consistent with the turnover time of SOC which were reported to be more than >100 years (Hemingway et al., 2019), and corroborates with the convergent view that persistence of SOC in soil is due to its accessibility to microbes rather than its molecular complexity (Lehmann et al., 2020; Schmidt et al., 2011).

4. Conclusions

Image analysis and numerical simulation of archived soil aggregates from a reversion experiment showed that converting plots that had been fallow for more than 70 years into wheat or grass gradually enhanced pore connectedness of the aggregates, but did not show noticeable changes in their ability to transport substrates in the first four years. A noticeable change started to emerge from the sixth year, especially the grass treatment, and became significant after 10 years; both porosity and bulk diffusion coefficient of the aggregates did not show signs of plateauing over the 10-year period. The diffusion coefficient of the aggregates is closely related to SOC at significant level, but we cannot ascertain that this is a feedback interaction or cause-consequence interaction; porosity is also positively related to SOC but not at a significant level. This difference indicates that the ability of the pore spaces to transport substrates is more important than the habitat they provide to SOC stabilisation. We also found that the conversion to grass not only increased numerate

connected pores but also rendered the intra-aggregate structures more geometrically different from that in the arable and bare fallow treatments.

Appendix

Substrate movement through the pore space in each aggregate was assumed to diffusive and simulated using the lattice Boltzmann model we developed previously as follows (Zhang et al., 2016a):

$$g_i\left(\boldsymbol{x}+\delta t\boldsymbol{e}_i, t+\delta t\right)=g_i\left(\boldsymbol{x},t\right)+\lambda\left[g_i^{eq}\left(\boldsymbol{x},t\right)-g_i\left(\boldsymbol{x},t\right)\right], \quad (1)$$

where $g_i\left(\boldsymbol{x},t\right)$ is particle distribution function at location $\boldsymbol{x}$ and time t moving with lattice velocity $\boldsymbol{e}_i$, $g_i^{eq}\left(\boldsymbol{x},t\right)$ is its associated equilibrium distribution function, λ is a dimensionless parameter and δt is time step. Since concentration is the only simulated variable, we used cubic lattice and allow the particle distribution functions to move in seven directions with lattice velocities $\left(0,\ 0,\ 0\right)$, $\left(\pm\delta x/\delta t,\ 0,\ 0\right)$, $\left(0,\ \pm\delta x/\delta t,\ 0\right)$ and $\left(0,\ 0,\ \pm\delta x/\delta t\right)$, where δx is the side-length of the voxels. The equilibrium distribution functions for all lattice velocities are the same, being $g_i^{eq}(\boldsymbol{x},t)=c\left(\boldsymbol{x},t\right)/7$, where $c(\boldsymbol{x},t)$ is the substrate concentration. During the simulation, the substrate concentration and diffusive flux $\boldsymbol{J}$ are calculated from:

$$\begin{aligned} c\left(\boldsymbol{x},t\right)&=\sum_{i=0}^{6}g_i\left(\boldsymbol{x},t\right),\\ \boldsymbol{J}(\boldsymbol{x},t)&=\left(1.0-0.5\lambda\right)\sum_{i=0}^{6}\boldsymbol{e}_i g_i(\boldsymbol{x},t). \end{aligned} \quad (2)$$

In the lattice Boltzmann model, molecular diffusion coefficient of the substrate, D, is related to time step and voxel size in $D=\delta x^2\left(1/\lambda-0.5\right)/3.5\delta t$.

Advancing one time step in the simulation needs two calculations. The first is to calculate the collision: $g_i^*=g_i\left(\boldsymbol{x},t\right)+\lambda\left[g_i^{eq}\left(\boldsymbol{x},t\right)-g_i\left(\boldsymbol{x},t\right)\right]$, and the second is to move g_i^* from $\boldsymbol{x}$ to $\boldsymbol{x}+\delta t\boldsymbol{e}_i$ at the end of the time step. Whenever g_i^* hits a pore wall during its movement, it is bounced back to where it emanates at the beginning of the time step to make the pore wall impermeable to the substrate.

Substrate concentration in all simulations was assumed to be zero everywhere, and its movement was initiated by a concentration gradient generated by imposing a high concentration C_1 on one side of the sample and a low concentration C_0 on its opposite side. We then simulated the substrate movement to steady state, after which we sampled its concentration and diffusive flux at all voxels to calculate the bulk diffusion coefficient and tortuosity using Eqs. (2) and (3) respectively.

Switching direction of the concentration gradient allows us to calculate the tortuosity and bulk diffusion coefficient in all three directions of a sample.

Acknowledgements

FW receives funding from the National Natural Science Foundation of China (project no. 51790535) and the Basic Scientific Research Project funded by Chinese Academy of Agricultural Sciences (Grant No. FIRI201606). The work at Rothamsted forms part of the soil to nutrition (S2N) strategic programme (BBS/E/C/000I0301) funded by the Biotechnology and Biological Sciences Research Council (BBSRC) of the UK. It is also funded by the Natural Environmental Research Council of the UK (NE/T010487/1). The Rothamsted Long-Term Experiments and the Electronic Rothamsted Archive (e-RA) are supported as a BBSRC-funded National Capability (BBS/E/C/000J0300).

References

Ananyeva, K., Wang, W., Smucker, A.J.M., Rivers, M.L., Kravchenko, A.N., 2013. Can intra-aggregate pore structures affect the aggregate's effectiveness in protecting carbon? Soil Biol. Biochem. 57, 868-875.

Angst, S., Mueller, C.W., Cajthaml, T., Angst, G., Lhotakova, Z., Bartuska, M., et al., 2017. Stabilization of soil organic matter by earthworms is connected with physical protection rather than with chemical changes of organic matter. Geoderma 289, 29-35.

Atkinson, J.A., Hawkesford, M.J., Whalley, W.R., Zhou, H., Mooney, S.J., 2020. Soil strength influences wheat root interactions with soil macropores. Plant Cell Environ. 43, 235-245.

Bacq-Labreuil, A., Crawford, J., Mooney, S.J., Neal, A.L., Akkari, E., McAuliffe, C., et al., 2018. Effects of cropping systems upon the three-dimensional architecture of soil systems are modulated by texture. Geoderma 332, 73-83.

Bacq-Labreuil, A., Crawford, J., Mooney, S.J., Neal, A.L., Ritz, K., 2020. Recovery of soil structure under long-term fallow in response to annual or perennial cropping requires at least 10 years after conversion. Enropean Journal of Soil Science 9, 9.

Bacq-Labreuil, A., Neal, A.L., Crawford, J., Mooney, S.J., Akkari, E., Zhang, X., et al., 2021. Significant structural evolution of a long-term fallow soil in response to agricultural management practices requires at least 10 years after conversion. Eur. J. Soil Sci. 72, 829-841.

Bauer, J., Herbst, M., Huisman, J.A., Weihermuller, L., Vereecken, H., 2008. Sensitivity of simulated soil heterotrophic respiration to temperature and moisture reduction functions. Geoderma 145, 17-27.
Bhattacharyya, R., Rabbi, S.M.F., Zhang, Y.Q., Young, I.M., Jones, A.R., Dennis, P.G., et al., 2021. Soil organic carbon is significantly associated with the pore geometry, microbial diversity and enzyme activity of the macro-aggregates under different land uses. Sci. Total Environ. 778, 10.
Christensen, B.T., 2001. Physical fractionation of soil and structural and functional complexity in organic matter turnover. Eur. J. Soil Sci. 52, 345-353.
Cooper, H.V., Sjogersten, S., Lark, R.M., Mooney, S.J., 2021. To till or not to till in a temperate ecosystem? Implications for climate change mitigation. Environ. Res. Lett. 16, 15.
Crawford, J.W., Deacon, L., Grinev, D., Harris, J.A., Ritz, K., Singh, B.K., et al., 2012. Microbial diversity affects self-organization of the soil-microbe system with consequences for function. J. R. Soc. Interface 9, 1302-1310.
Davidson, E.A., Verchot, L.V., Cattanio, J.H., Ackerman, I.L., Carvalho, J.E.M., 2000. Effects of soil water content on soil respiration in forests and cattle pastures of eastern Amazonia. Biogeochemistry 48, 53-69.
De Gryze, S., Jassogne, L., Six, J., Bossuyt, H., Wevers, M., MerckX, R., 2006. Pore structure changes during decomposition of fresh residue: X-ray tomography analyses. Geoderma 134, 82-96.
Dungait, J.A.J., Hopkins, D.W., Gregory, A.S., Whitmore, A.P., 2012. Soil organic matter turnover is governed by accessibility not recalcitrance. Glob. Change Biol. 18, 1781-1796.
Gillabel, J., Cebrian-Lopez, B., Six, J., Merckx, R., 2010. Experimental evidence for the attenuating effect of SOM protection on temperature sensitivity of SOM decomposition. Glob. Change Biol. 16, 2789-2798.
Gregory, A.S., Dungait, J.A.J., Watts, C.W., Bol, R., Dixon, E.R., White, R.P., et al., 2016. Long-term management changes topsoil and subsoil organic carbon and nitrogen dynamics in a temperate agricultural system. Eur. J. Soil Sci. 67, 421-430.
Guo, Y.F., Fan, R.Q., Zhang, X.P., Zhang, Y., Wu, D.H., McLaughlin, N., et al., 2020. Tillage-induced effects on SOC through changes in aggregate stability and soil pore structure. Sci. Total Environ. 703, 9.
Helliwell, J.R., Miller, A.J., Whalley, W.R., Mooney, S.J., Sturrock, C.J., 2014. Quantifying the impact of microbes on soil structural development and behaviour in wet soils. Soil Biology and Biochemistry 74, 138-147.
Hemingway, J.D., Rothman, D.H., Grant, K.E., Rosengard, S.Z., Eglinton, T.I., Derry, L.A., et al., 2019. Mineral protection regulates long-term global preservation of natural organic carbon. Nature 570, 228-+.
Hirsch, P.R., Jhurreea, D., Williams, J.K., Murray, P.J., Scott, T., Misselbrook, T.H., et al., 2017. Soil resilience and recovery: rapid community responses to management changes. Plant Soil 412, 283-297.
Hursh, A., Ballantyne, A., Cooper, L., Maneta, M., Kimball, J., Watts, J., 2017. The sensitivity of soil respiration to soil temperature, moisture, and carbon supply at the global scale. Glob. Change Biol. 23, 2090-2103.
Jastrow, J.D., Boutton, T.W., Miller, R.M., 1996. Carbon dynamics of aggregate-associated organic matter estimated by carbon-13 natural abundance. Soil Sci. Soc. Am. J. 60, 801-807.
Jensen, J.L., Schjønning, P., Watts, C.W., Christensen, B.T., Obour, P.B., Munkholm, L.J., 2020. Soil degradation and recovery – Changes in organic matter fractions and structural stability. Geoderma 364, 114181.
Jensen, J.L., Schjonning, P., Watts, C.W., Christensen, B.T., Peltre, C., Munkholm, L.J., 2019. Relating soil C and organic matter fractions to soil structural stability. Geoderma 337, 834-843.
John, B., Yamashita, T., Ludwig, B., Flessa, H., 2005. Storage of organic carbon in aggregate and density fractions of silty soils under different types of land use. Geoderma 128, 63-79.

Johnston, A.E., Poulton, P.R., Coleman, K., 2009. Chapter 1 Soil Organic Matter: Its Importance in Sustainable Agriculture and Carbon Dioxide Fluxes, In: Sparks, D.L. (Ed.), Advances in Agronomy. Academic Press, pp. 1-57.
Juarez, S., Nunan, N., Duday, A.C., Pouteau, V., Schmidt, S., Hapca, S., et al., 2013. Effects of different soil structures on the decomposition of native and added organic carbon. Eur. J. Soil Biol. 58, 81-90.
Kallenbach, C.M., Frey, S.D., Grandy, A.S., 2016. Direct evidence for microbial-derived soil organic matter formation and its ecophysiological controls. Nat. Commun. 7, 10.
Keiluweit, M., Nico, P.S., Kleber, M., Fendorf, S., 2016. Are oxygen limitations under recognized regulators of organic carbon turnover in upland soils? Biogeochemistry 127, 157-171.
Kravchenko, A., Otten, W., Garnier, P., Pot, V., Baveye, P.C., 2019a. Soil aggregates as biogeochemical reactors: Not a way forward in the research on soil-atmosphere exchange of greenhouse gases. Glob. Change Biol. 25, 2205-2208.
Kravchenko, A.N., Guber, A.K., Razavi, B.S., Koestel, J., Quigley, M.Y., Robertson, G.P., et al., 2019b. Microbial spatial footprint as a driver of soil carbon stabilization. Nat. Commun. 10, 10.
Lehmann, J., Hansel, C.M., Kaiser, C., Kleber, M., Maher, K., Manzoni, S., et al., 2020. Persistence of soil organic carbon caused by functional complexity. Nature Geoscience 13, 529-534.
Li, Z.Y., Zhang, X.X., Wang, D., Liu, Y., 2018. Direct methods to calculate the mass exchange between solutes inside and outside aggregates in macroscopic model for solute transport in aggregated soil. Geoderma 320, 126-135.
Lobe, I., Sandhage-Hofmann, A., Brodowski, S., du Preez, C.C., Amelung, W., 2011. Aggregate dynamics and associated soil organic matter contents as influenced by prolonged arable cropping in the South African Highveld. Geoderma 162, 251-259.
Naveed, M., Arthur, E., de Jonge, L.W., Tuller, M., Moldrup, P., 2014. Pore Structure of Natural and Regenerated Soil Aggregates: An X-Ray Computed Tomography Analysis. Soil Sci. Soc. Am. J. 78, 377-386.
Neal, A.L., Bacq-Labreuil, A., Zhang, X.X., Clark, I.M., Coleman, K., Mooney, S.J., et al., 2020. Soil as an extended composite phenotype of the microbial metagenome. Sci Rep 10, 16.
Neuman, S.P., 1990. UNIVERSAL SCALING OF HYDRAULIC CONDUCTIVITIES AND DISPERSIVITIES IN GEOLOGIC MEDIA. Water Resour. Res. 26, 1749-1758.
Nunan, N., Wu, K.J., Young, I.M., Crawford, J.W., Ritz, K., 2003. Spatial distribution of bacterial communities and their relationships with the micro-architecture of soil. FEMS Microbiol. Ecol. 44, 203-215.
Pabst, W., Gregorova, E., 2006. A new percolation-threshold relation for the porosity dependence of thermal conductivity. Ceramics International 32, 89-91.
Perryman, S.A.M., Castells-Brooke, N.I.D., Glendining, M.J., Goulding, K.W.T., Hawkesford, M.J., Macdonald, A.J., et al., 2018. The electronic Rothamsted Archive (e-RA), an online resource for data from the Rothamsted long-term experiments. Sci. Data 5, 17.
Rabbi, S.M.F., Daniel, H., Lockwood, P.V., Macdonald, C., Pereg, L., Tighe, M., et al., 2016. Physical soil architectural traits are functionally linked to carbon decomposition and bacterial diversity. Sci Rep 6, 9.
Rabbi, S.M.F., Minasny, B., McBratney, A.B., Young, L.M., 2020. Microbial processing of organic matter drives stability and pore geometry of soil aggregates. Geoderma 360, 4.
Rabbi, S.M.F., Tighe, M.K., Flavel, R.J., Kaiser, B.N., Guppy, C.N., Zhang, X.X., et al., 2018. Plant roots redesign the rhizosphere to alter the three-dimensional physical architecture and water dynamics. New Phytol. 219, 542-550.
Redmile-Gordon, M., Gregory, A.S., White, R.P., Watts, C.W., 2020. Soil organic carbon, extracellular polymeric substances (EPS), and soil structural stability as affected by previous and current land-use. Geoderma 363, 10.
Sainte-Marie, J., Barrandon, M., Saint-André, L., Gelhaye, E., Martin, F., Derrien, D., 2021. C-STABILITY an innovative modeling framework to leverage the continuous representation of organic matter. Nat. Commun. 12, 810.

555 Schmidt, M.W.I., Torn, M.S., Abiven, S., Dittmar, T., Guggenberger, G., Janssens, I.A., et al., 2011.
556 Persistence of soil organic matter as an ecosystem property. Nature 478, 49-56.
557 Six, J., Elliott, E.T., Paustian, K., 2000. Soil macroaggregate turnover and microaggregate formation: a
558 mechanism for C sequestration under no-tillage agriculture. Soil Biol. Biochem. 32, 2099-2103.
559 Skopp, J., Jawson, M.D., Doran, J.W., 1990. Steady-state aerobic microbial activity as a function of
560 soil water content Soil Sci. Soc. Am. J. 54, 1619-1625.
561 Tisdall, J.M., Oades, J.M., 1982. Organic matters and water-stable aggregates in soils Journal of Soil
562 Science 33, 141-163.
563 Totsche, K.U., Amelung, W., Gerzabek, M.H., Guggenberger, G., Klumpp, E., Knief, C., et al., 2018.
564 Microaggregates in soils. J. Plant Nutr. Soil Sci. 181, 104-136.
565 Tripathi, R., Nayak, A.K., Bhattacharyya, P., Shukla, A.K., Shahid, M., Raja, R., et al., 2014. Soil
566 aggregation and distribution of carbon and nitrogen in different fractions after 41 years long-term
567 fertilizer experiment in tropical rice-rice system. Geoderma 213, 280-286.
568 Wang, B., Brewer, P.E., Shugart, H.H., Lerdau, M.T., Allison, S.D., 2019. Soil aggregates as
569 biogeochemical reactors and implications for soil-atmosphere exchange of greenhouse gases-A
570 concept. Glob. Change Biol. 25, 373-385.
571 Wang, L., Xiong, X., Luo, X.S., Chen, W.L., Wen, S.L., Wang, B.R., et al., 2020. Aggregational
572 differentiation of ureolytic microbes in an Ultisol under long-term organic and chemical fertilizations.
573 Sci. Total Environ. 716, 7.
574 Wiesmeier, M., Urbanski, L., Hobley, E., Lang, B., von Lutzow, M., Marin-Spiotta, E., et al., 2019. Soil
575 organic carbon storage as a key function of soils - A review of drivers and indicators at various scales.
576 Geoderma 333, 149-162.
577 Yan, Z.F., Bond-Lamberty, B., Todd-Brown, K.E., Bailey, V.L., Li, S.L., Liu, C.Q., et al., 2018. A moisture
578 function of soil heterotrophic respiration that incorporates microscale processes. Nat. Commun. 9,
579 10.
580 Yang, J.Q., Zhang, X., Bourg, I.C., Stone, H.A., 2021. 4D imaging reveals mechanisms of clay-carbon
581 protection and release. Nat. Commun. 12, 622.
582 Young, I.M., Crawford, J.W., 2004. Interactions and self-organization in the soil-microbe complex.
583 Science 304, 1634-1637.
584 Zhang, X., Crawford, J.W., Flavel, R.J., Young, I.M., 2016a. A multi-scale Lattice Boltzmann model for
585 simulating solute transport in 3D X-ray micro-tomography images of aggregated porous materials. J.
586 Hydrol. 541, Part B, 1020-1029.
587 Zhang, X., Neal, A.L., Crawford, J.W., Bacq-Labreuil, A., Akkari, E., Rickard, W., 2021a. The effects of
588 long-term fertilizations on soil hydraulic properties vary with scales. J. Hydrol. 593, 125890.
589 Zhang, X.X., Crawford, J.W., Young, I.M., 2016b. A Lattice Boltzmann model for simulating water flow
590 at pore scale in unsaturated soils. J. Hydrol. 538, 152-160.
591 Zhang, Y., Yang, Z., Wang, F., Zhang, X., 2021b. Comparison of soil tortuosity calculated by different
592 methods. Geoderma 402, 115358.
593 Zhou, H., Peng, X.H., Perfect, E., Xiao, T.Q., Peng, G.Y., 2013. Effects of organic and inorganic
594 fertilization on soil aggregation in an Ultisol as characterized by synchrotron based X-ray micro-
595 computed tomography. Geoderma 195, 23-30.
596 Zhou, H., Whalley, W.R., Hawkesford, M.J., Ashton, R.W., Atkinson, B., Atkinson, J.A., et al., 2020.
597 The interaction between wheat roots and soil pores in structured field soil. J. Exp. Bot. 72, 747-756.

598

599

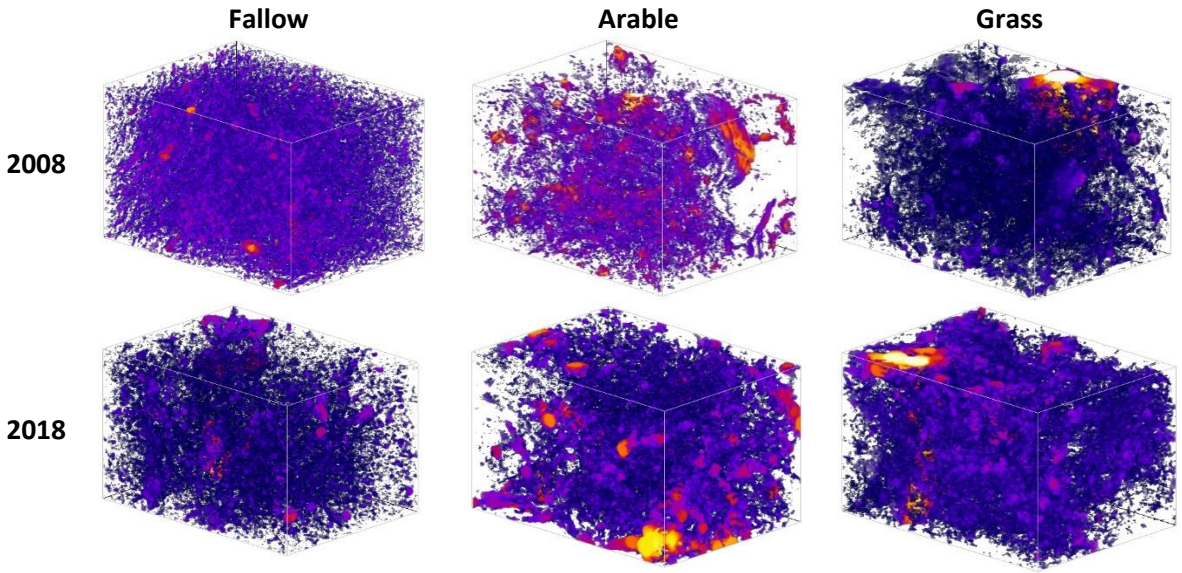

Figure 1. Samples selected randomly from each treatment to illustrate the change in intra-aggregate pore geometry. In 2008 (the top panel). In 2018,10 years after the conversion (the bottom panel). In all images, pore size increases from dark to bright and the solid phase was made transparent.

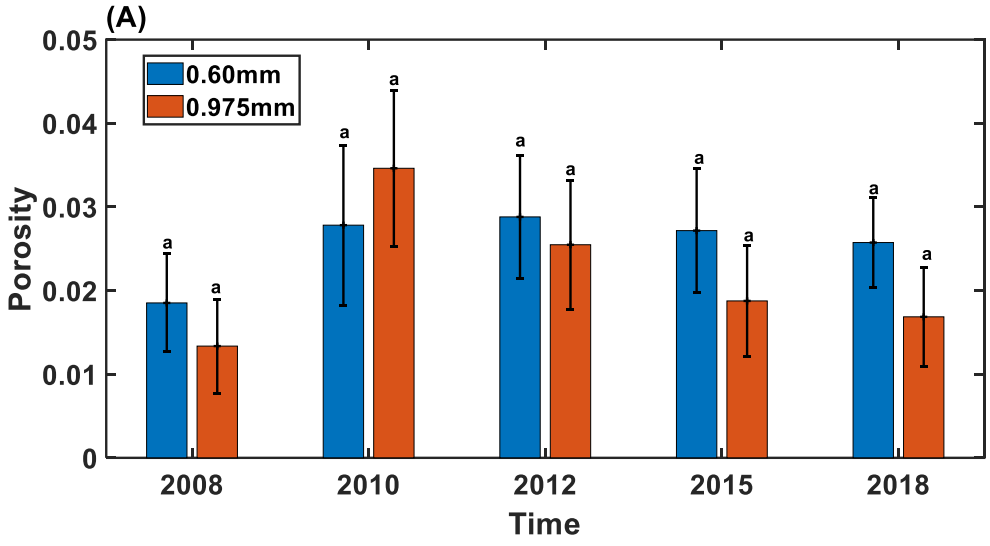

607

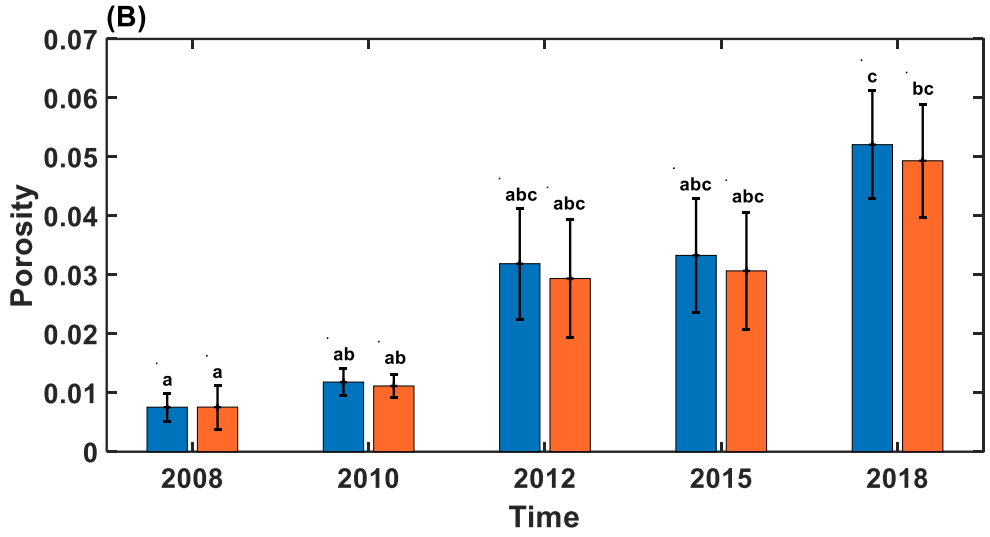

608

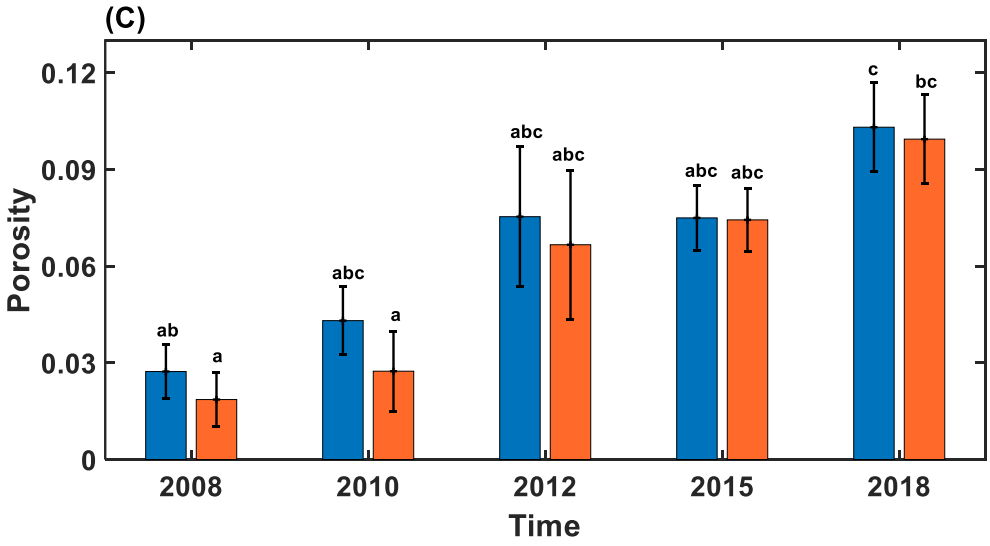

609

610 **Figure 2**. Change in volumetric fraction of the connected pores in the pore clusters
611 stretching to 0.60mm and 0.975mm respectively, as time elapsed after the conversion in
612 2008. (A) Continuous bare fallow; (B) conversion from fallow to arable; (C) conversion from
613 fallow to grass. The lowercase letters represent significant difference at $p<0.05$.

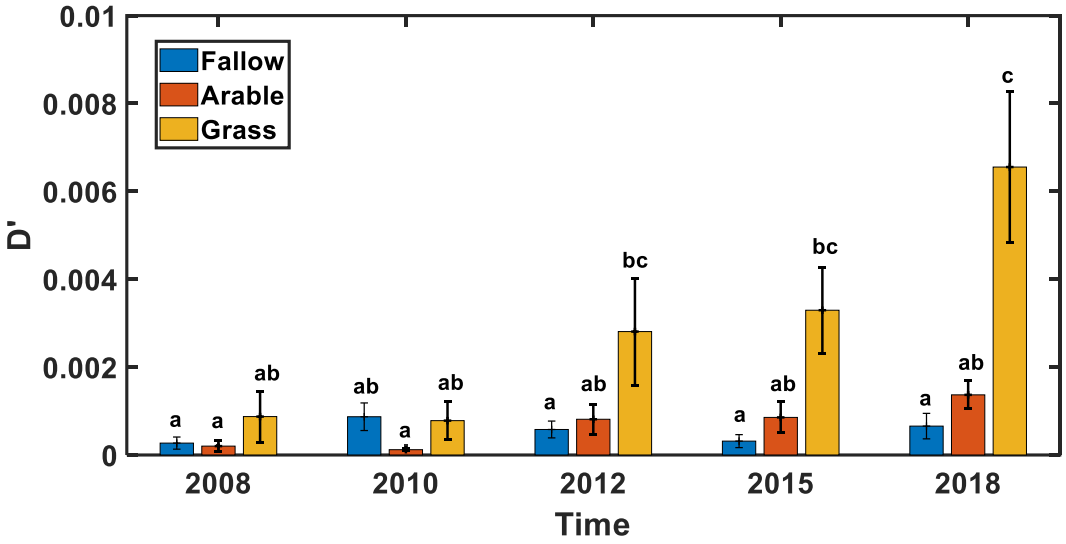

Figure 3. Change in normalized bulk diffusion coefficient (D') of the aggregates in each of the three treatments as the time elapsed after the conversion in 2008. The lowercase letters represent significant difference at $p<0.05$.

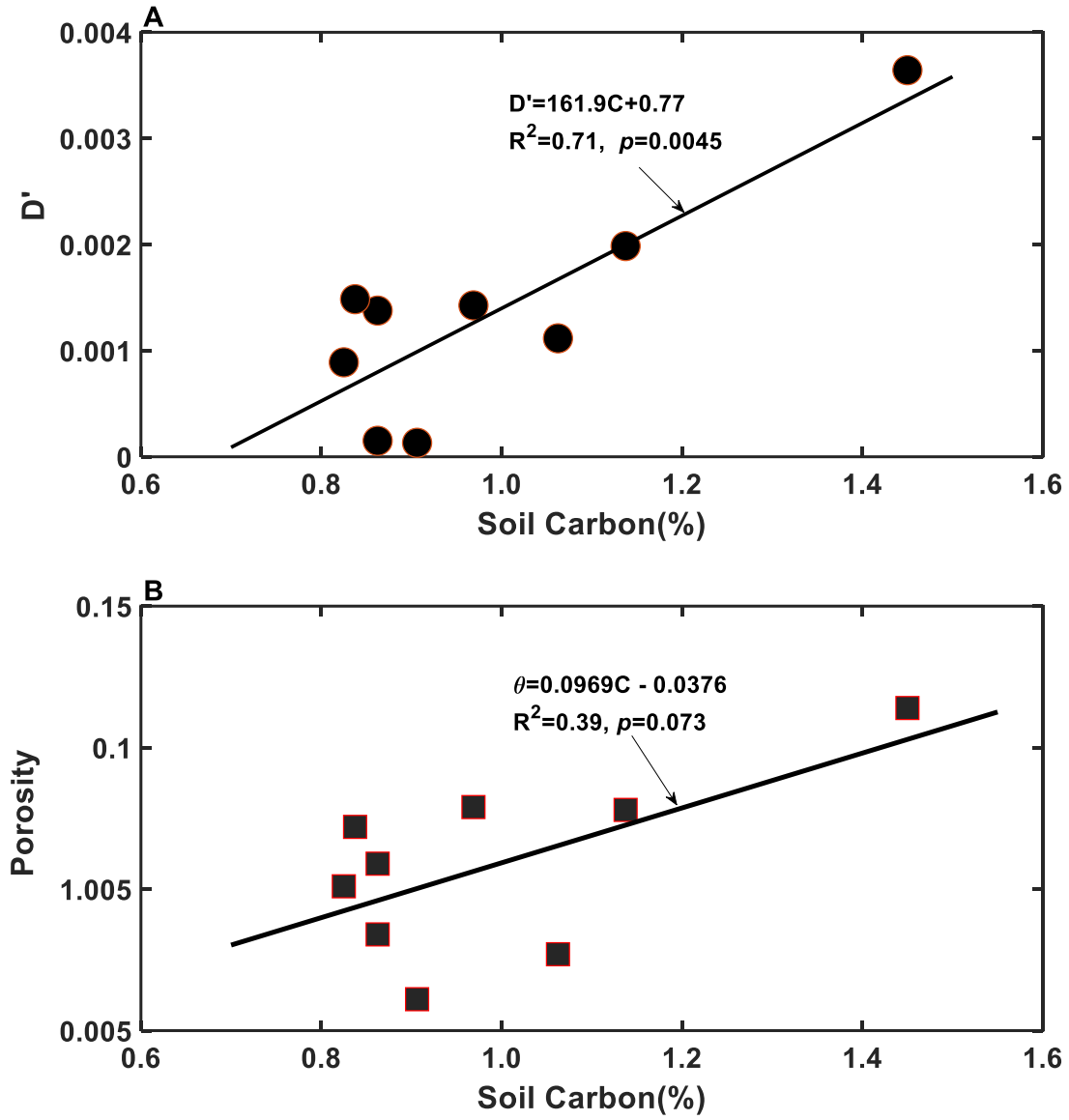

Figure 4. Relationship between SOC (percentage in weight) and the normalized average bulk diffusion coefficient (A); between SOC and the volumetric fraction of connected pores (B), for all treatments over the 10-year period.

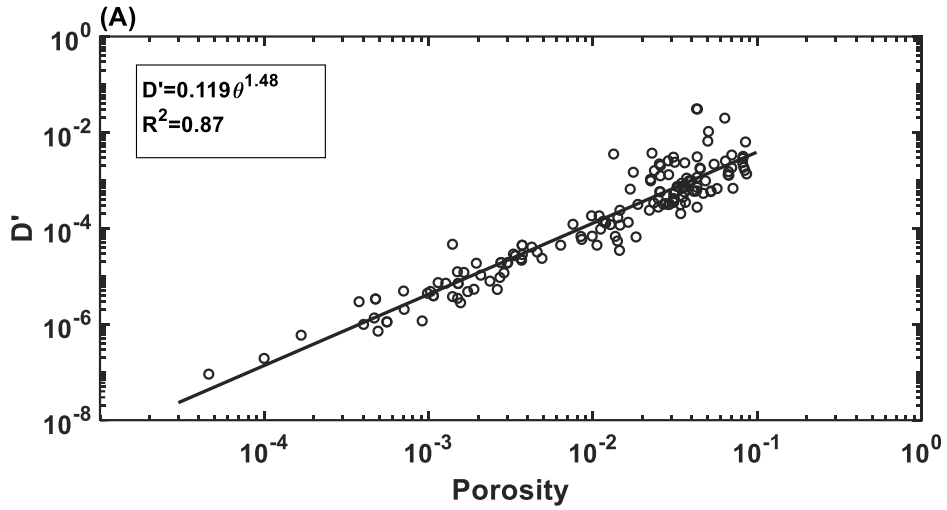

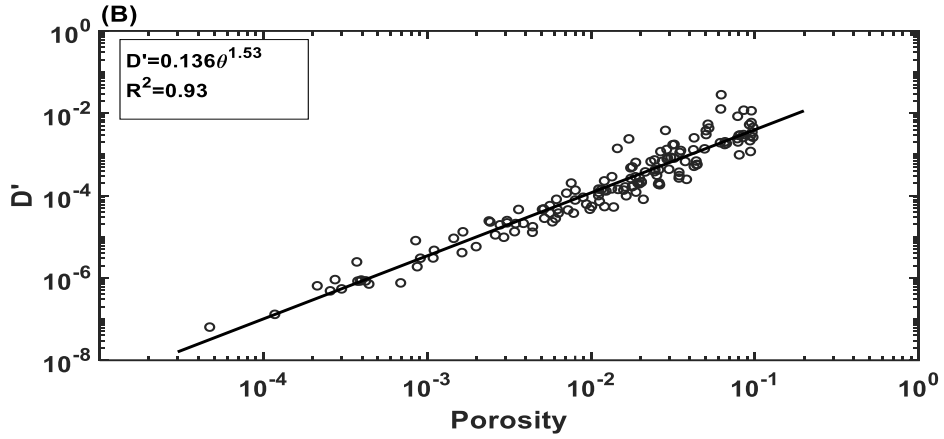

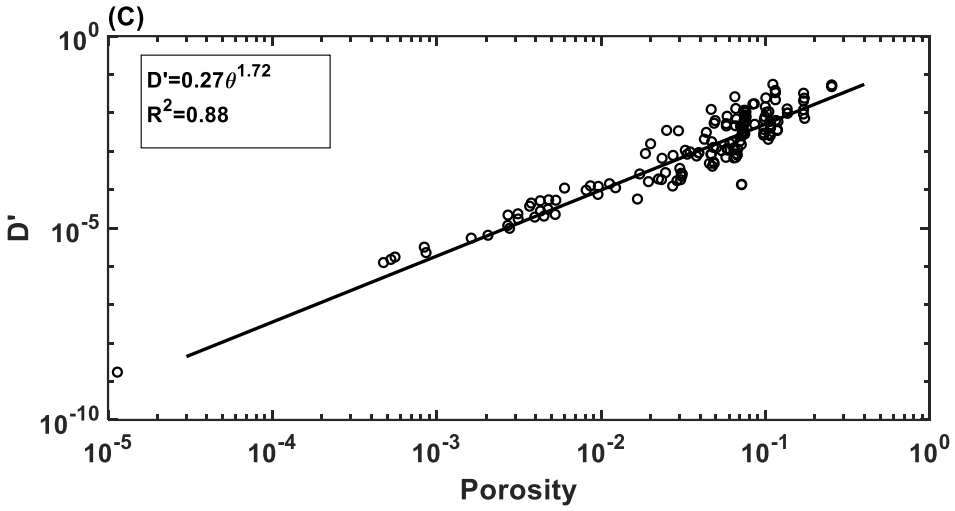

Figure 5. Change in the normalized bulk diffusion coefficient (D') with porosity (including connected pores only) for all aggregates in different treatments. (A) Continuous bare fallow; (B) conversion from fallow to arable; (C) conversion from fallow to grassland. The regression curve for the grass treatment differs significantly from the regression curves for the other two treatments.

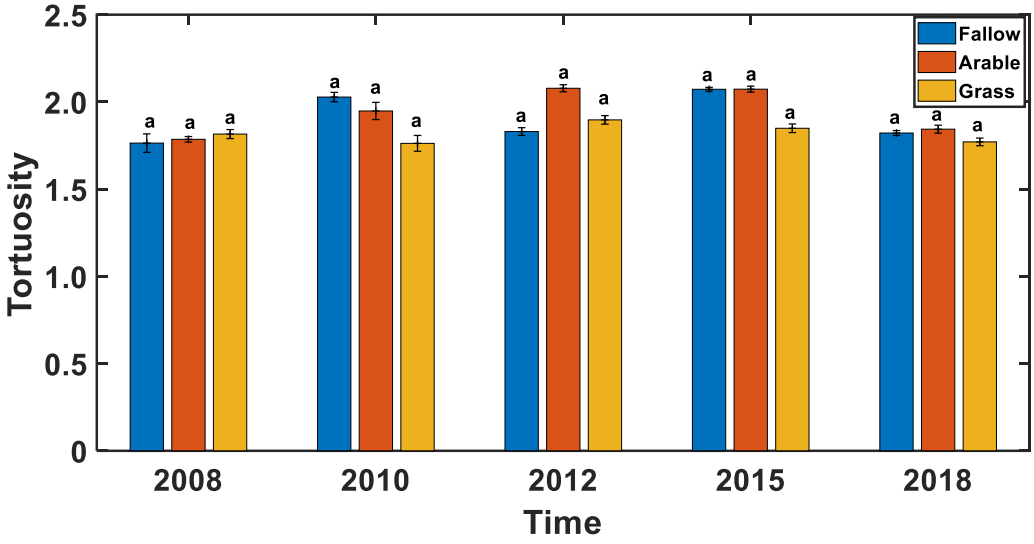

641

642 **Figure 6**. Change in tortuosity (average + standard errors) of aggregates with time for all
643 three treatments. The lowercase letters represent significant difference at $p<0.05$.

644